Supporting Information

Plasma surface functionalization induces nanostructure and nitrogen-doping in carbon cloth with enhanced energy storage performance

Bo Ouyang,[a] Yongqi Zhang,[b] Ying Wang,[a,c] Zheng Zhang,[d] Hong Jin Fan* [b], and Rajdeep Singh Rawat* [a]

---

[a] *Natural Sciences and Science Education, National Institute of Education, Nanyang Technological University, 637616, Singapore*
email: rajdeep.rawat@nie.edu.sg
[b] *School of Physical and Mathematical Sciences, Nanyang Technological University, Singapore 637371, Singapore*
email: fanhj@ntu.edu.sg
[c] *School of Materials Science and Engineering, Nanyang Technological University, Singapore 639798, Singapore*
[d] *Institute of Materials Research and Engineering, A*STAR (Agency for Science, Technology and Research), #08-03, Fusionopolis Way, Innovis, 138634, Singapore*

B. Ouyang and Y. Q. Zhang contributed equally to this work.

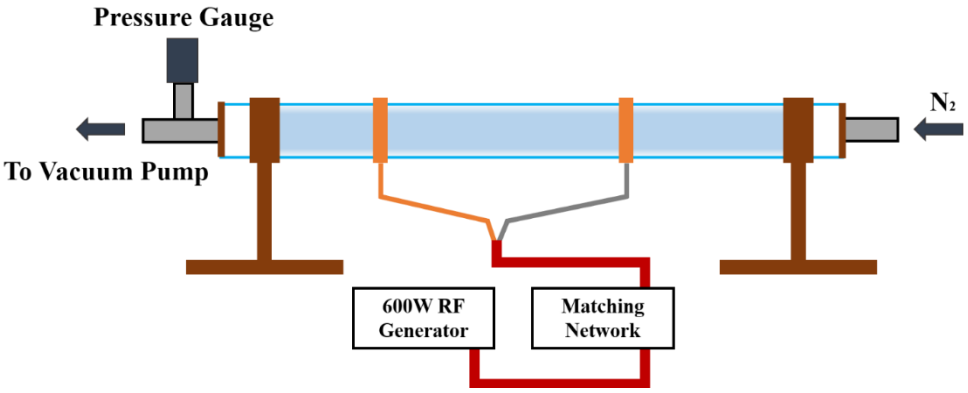

Figure S1: Schematic diagram of home-made RF plasma system.

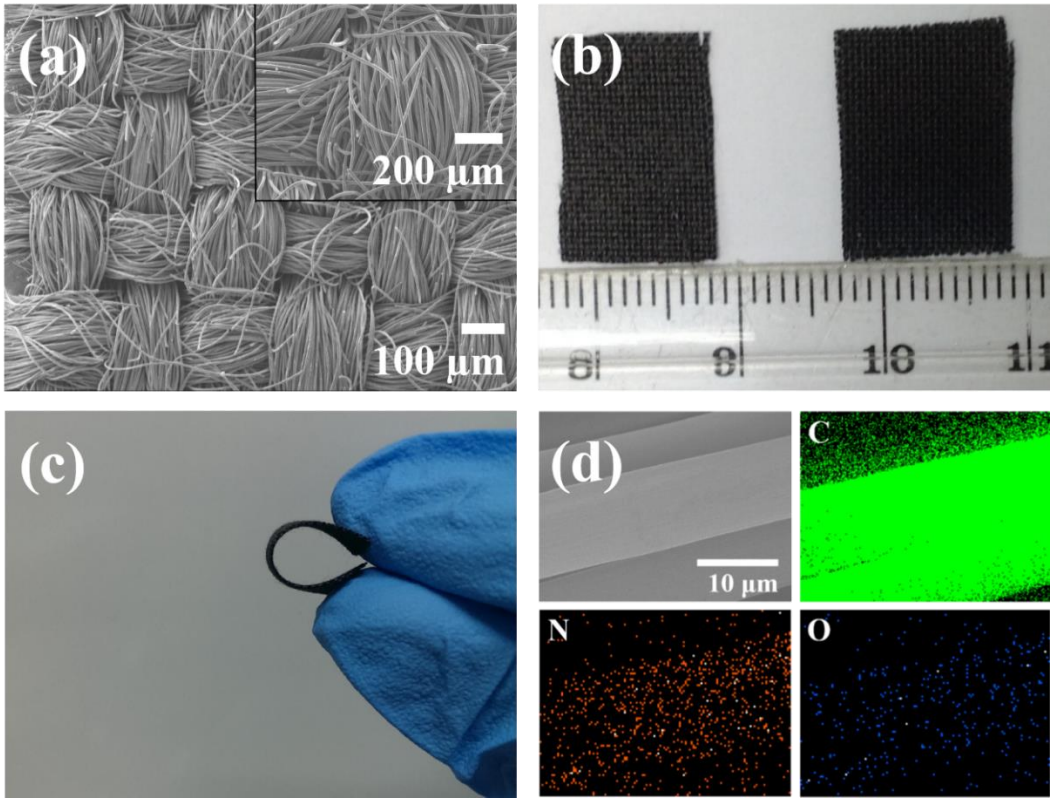

Figure S2: (a) SEM of untreated CC; (b) digital photo of the untreated CC (left) and the hNCC sample (right); (c) Digital photos for illustrating the excellent flexibility of the hNCC sample; (d) EDS mapping of C, N, O for hNCC sample.

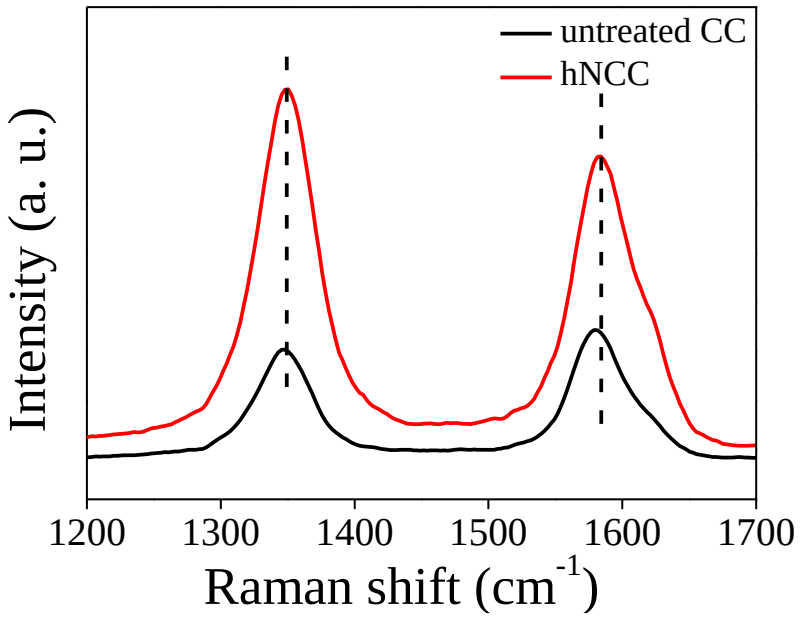

Figure S3: Raman spectra of the hNCC and untreated CC.

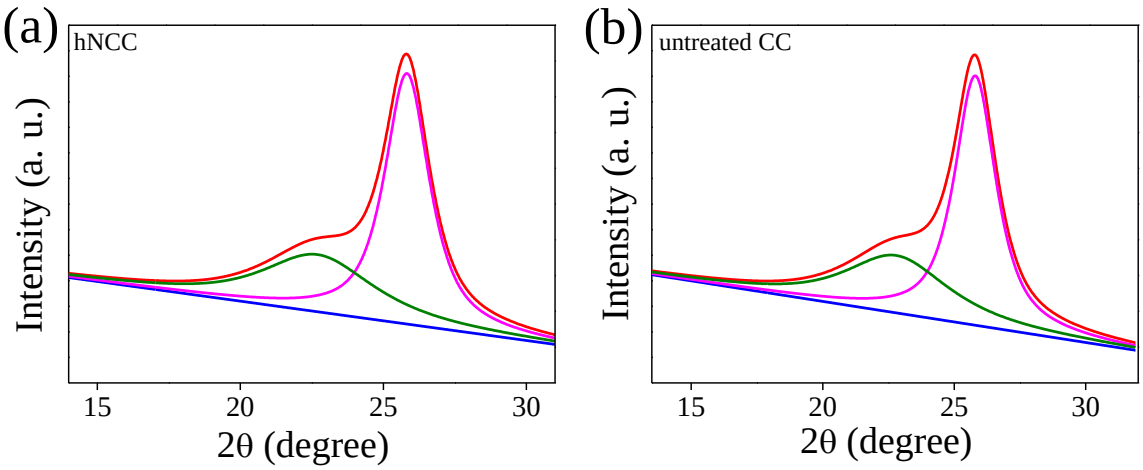

Figure S4: (a) XRD pattern of hNCC; (b) XRD pattern of untreated CC sample.

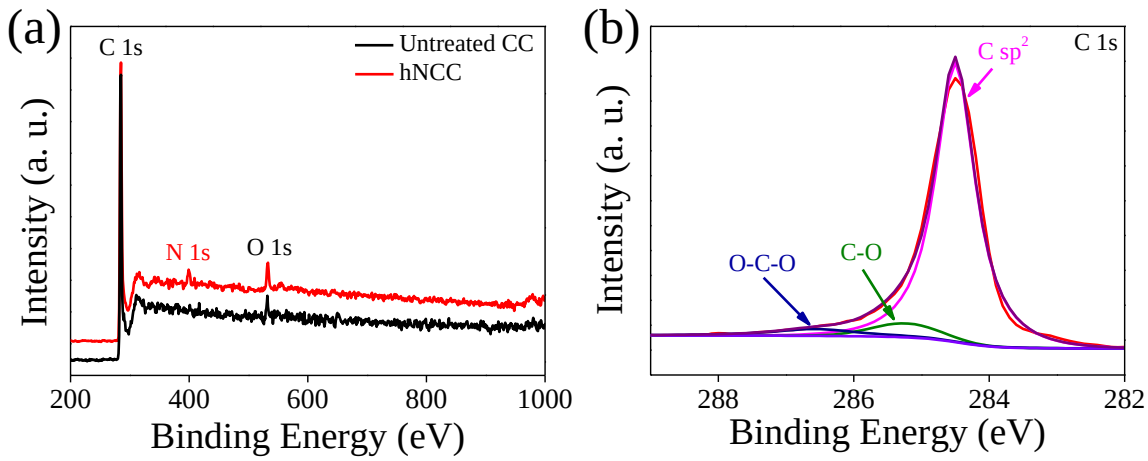

Figure S5: (a) XPS spectra of hNCC and untreated CC; (b) High resolution XPS spectra of C1 in untreated CC.

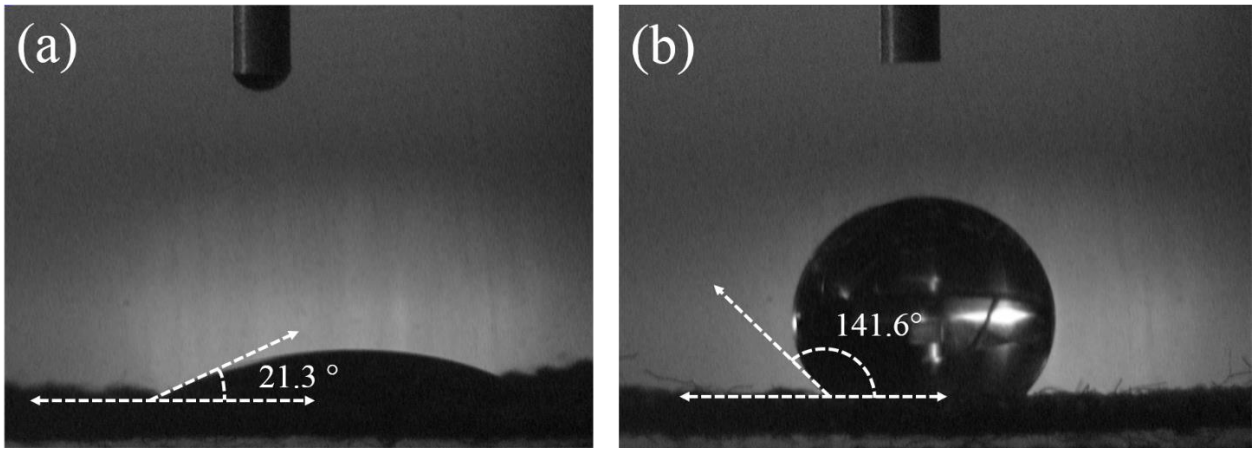

Figure S6: Water contact angle measurement for the hNCC and untreated CC after resting the water droplet on the surface for 5 s.

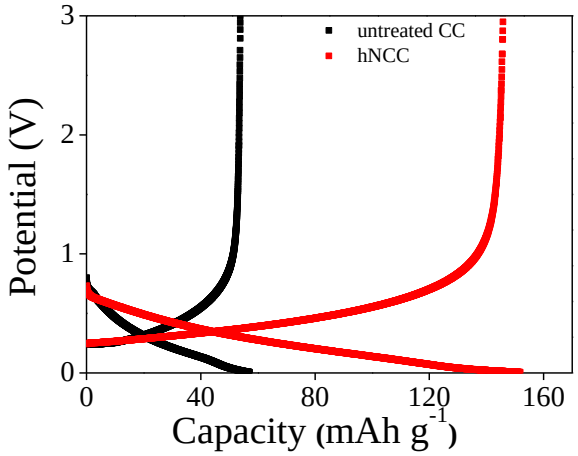

Figure S7: initial galvanostatic charge-discharge voltage versus capacity profiles of hNCC and untreated CC samples at a current density of 100 mA g^{-1}.

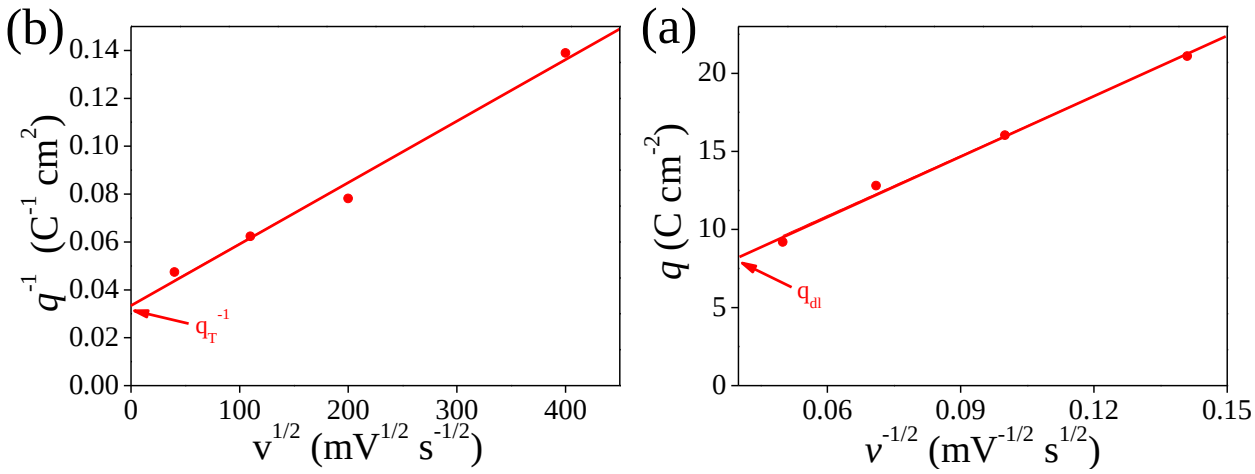

Figure S8: (a) Dependence of $1/q$ on $v^{1/2}$ and (b) dependence of q on $v^{-1/2}$ for hNCC.

Differentiate the pseudocapacitance and double-layer capacitance contributions:

Because of the similar double-layer current density between hNCC and pristine CC as well as their similar material characteristics, the capacitive performance differences can be ascribed to the presence of nitrogen-containing functional groups. Hence, it can be possible to compare the respective contribution of pseudocapacitance from hNCC. Due to the relatively slower electrochemical kinetics of the redox couples coming from N-containing functional groups compared to the double-layer process, the specific capacitance is proposed to be partitioned into

double-layer capacitance and pseudocapacitance. In the partition procedure, the total voltammetric charge, q_T, can be estimated from the extrapolation of voltammetric charge, q to v = 0 from the plot of $1/q$ vs. $v^{1/2}$ (Figure S8a). The double-layer charge, q_{dl}, is given from the extrapolation of q to $v = \infty$ from the plot of q vs. $v^{-1/2}$ (Figure S8b). Accordingly, the pseudocapacitance charge, q_p, can be obtained from the difference between q_T and q_{dl}.

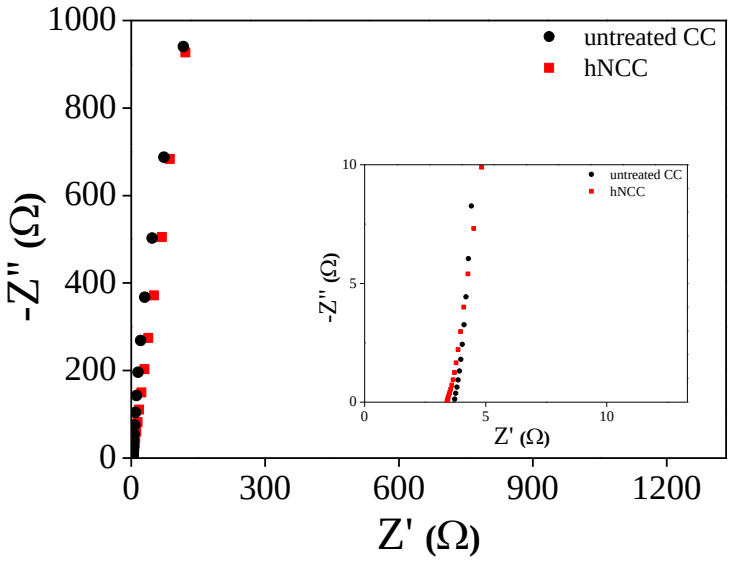

Figure S9: EIS spectra of hNCC and untreated CC at high frequency.

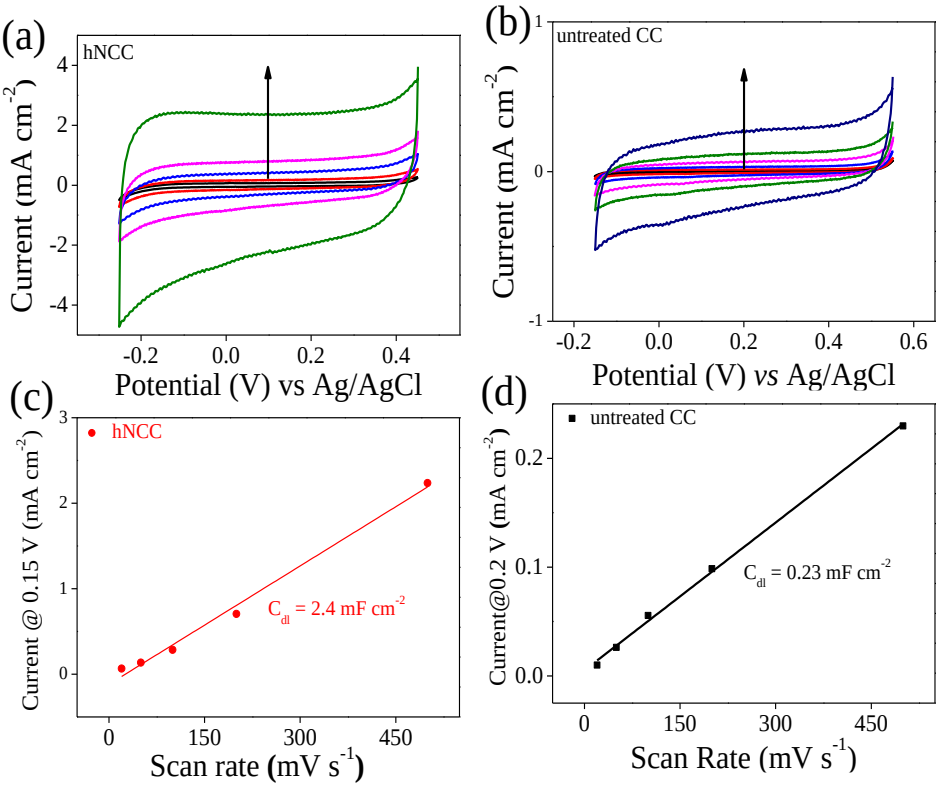

Figure S10: (a) typical voltammograms of hNCC measured in 1 M NaOH; (b) typical volatmmograms of untreated CC measured in NaOH; (c) average capacitive current of hNCC taken from center of potential window at 0.15 V vs. Ag/AgCl; (d) average capacitive current of untreated CC taken from center of potential window at 0.2 V vs. Ag/AgCl.

The estimation of the effective active surface area of the samples was carried out according to literature. Cyclic voltammetry (CV) of hNCC were performed at various scan rates (20, 50, 100, 200 and 500 mV s^{-1}) in -0.25 – 0.45 V vs. RHE region (Figure S10a). The double-layer capacitance (C_{dl}) of various samples can be determined from the cyclic voltammograms, which is expected to be linearly proportional to the effective surface area. CV measurements of hNCC were taken into the region of -0.25 – 0.45 V while that of untreated CC in the region of -0.15 – 0.55 V (Figure S10b), which could be mostly considered as the double-layer capacitive behavior. The double-layer capacitance is estimated at 0.15 V vs. Ag/AgCl against the scan rate, where the slop is twice of that of C_{dl} (Figure S10c and Figure S10d). The calculated values of double-layer

capacitance are 2.4 mF cm^{-2} and 0.23 mF cm^{-2} for the hNCC and untreated CC, respectively. Since the C_{dl} is proportional to the surface area of the materials, the ratio of the C_{dl} can be regarded as the ratio of the electrochemical surface area. According to the results, the C_{dl} ratio of hNCC to untreated CC is estimated to be 10:1, indicating much larger surface area of hNCC as compared to untreated CC. It should be noted that the surface area determined by electrochemical capacitance measurements was found to depend on pH; specifically, the measured surface area increases with pH, likely due to the greater number of OH^- ions present when charging the film-electrolyte interface. As such, all roughness factors were determined using data collected under the same conditions (1M NaOH). In addition, an inherent assumption when using electrochemical capacitance methods is that the nature of charging in hNCC and untreated CC samples is not dependent on these compositions. That is, we neglect any changes in the capacitance due to movement of ions within samples. These observations imply that the measured surface area is not an absolute value but a relative value.

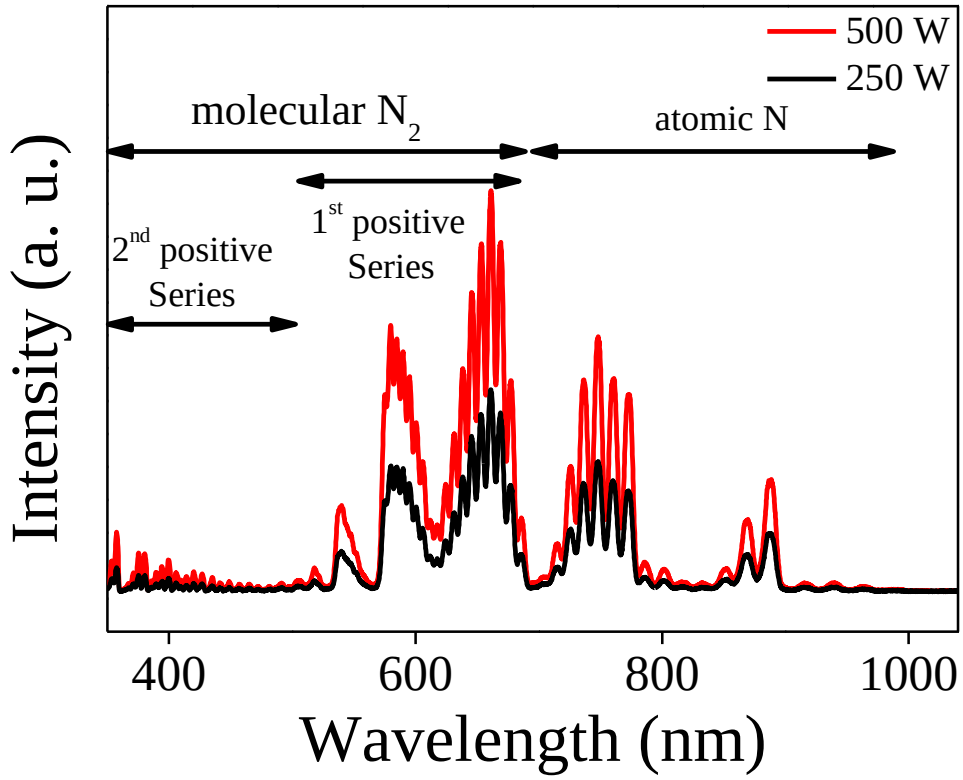

Figure S11: OES spectra of nitrogen plasma at different power density.

Table S1 percentages of different nitrogen contents in hNCC and rNCC.

Functional groups	N-Q	N-5	N-6	N-X
hNCC	6.31%	46.3%	39.8%	7.58%
rNCC	11.93%	22.07%	60.03%	5.97%

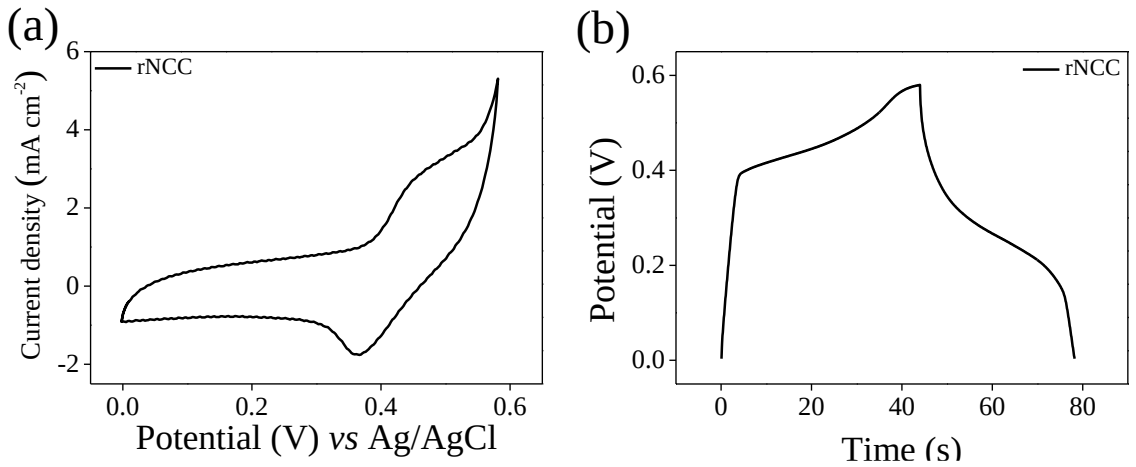

Figure S12: CV curve of rNCC at 200 mV s^{-1}; (b) GCD curve of rNCC at 4 mA cm^{-2}.

Table S2: Comparison of electrochemical performance for carbon-based composites.

system	C_s (current density)	Rate capability	Cycling stability	Reference
NG-PAA/PANI-CC[1]	521 F g^{-1} (0.5 A g^{-1})	75% (392 F g^{-1}, 10 A g^{-1})	83.2% (2000, 1 A g^{-1})	S1
GOCC[2]	702 mF cm^{-2} (1 mA cm^{-2})	86.9% (610 mF cm^{-2}, 20 mA cm^{-2})	110.5% (30000, 10 mA cm^{-2})	S2
CNTs/CC[3]	225 F g^{-1} (1 A g^{-1})	77% (173 F g-1, 5 A g^{-1})	90% (10000, 1 A g^{-1})	S3
Activated CC[4]	505 mF cm^{-2} (6 mA cm^{-2})	88% (445 mF cm^{-2}, 48 mA cm-2)	97% (10000, 24 mA cm^{-2})	S4
Fe_2O_3-CC[5]	180 mF cm^{-2} (1 mA cm-2)	75% (135 mF cm^{-2}, 10 mA cm^{-2})		S5
oxidized CC[6]	88 mF cm^{-2} (10 mV s^{-1})	76% (67 mF cm^{-2}, 1000 mV s^{-1})	97% (20000, 1000 mV s^{-1})	S6
N-CNT/CF2[7]	133.1 F g^{-1} (0.5 A g^{-1})	63.3% (84.3 F g^{-1}, 200 A g^{-1})	95% (5000, 50 A g^{-1})	S7
TiO_2@PPy[8]	56.2 mF cm^{-2} (0.3 mA cm^{-2})	55.2% (31 mF cm^{-2}, 8 mA cm^{-2})		S8
Porous RGO[9]	71 mF cm^{-2} (1 mA cm^{-2})	79% (56.1 mF cm^{-2}, 100 mA cm^{-2})	98.3% (5000, 10 mA cm^{-2})	S9
hNCC	159 mAh g^{-1} (0.1 A g^{-1}) 391 mF cm^{-2} (4 mA cm^{-2})	35% (55 mAh g^{-1}, 0.8 A g^{-1}) 39% (156 mF cm^{-2}, 40 mA cm^{-2})	~99% (100, 0.1 A g^{-1}) ~98% (10000, 4 mA cm^{-2})	This work

Reference

[1] Y. Wang, S. Tang, S. Vongehr, J. A. Syed, X. Wang, X. Meng, Scientific reports 2016, 6.

[2] S. Gao, L. Zhu, L. Liu, A. Gao, F. Liao, M. Shao, Electrochimica Acta 2016, 191, 908.

[3] Y.-K. Hsu, Y.-C. Chen, Y.-G. Lin, L.-C. Chen, K.-H. Chen, Journal of Materials Chemistry 2012, 22, 3383.

[4] D. Ye, Y. Yu, J. Tang, L. Liu, Y. Wu, Nanoscale 2016, 8, 10406.

[5] P. Yang, Y. Ding, Z. Lin, Z. Chen, Y. Li, P. Qiang, M. Ebrahimi, W. Mai, C. P. Wong, Z. L. Wang, Nano letters 2014, 14, 731.

[6] G. Wang, H. Wang, X. Lu, Y. Ling, M. Yu, T. Zhai, Y. Tong, Y. Li, Advanced materials 2014, 26, 2676.

[7] S. He, H. Hou, W. Chen, Journal of Power Sources 2015, 280, 678.

[8] M. Yu, Y. Zeng, C. Zhang, X. Lu, C. Zeng, C. Yao, Y. Yang, Y. Tong, Nanoscale 2013, 5, 10806.

[9] Z. Xiong, C. Liao, W. Han, X. Wang, Advanced materials 2015, 27, 4469.